Chemistry of Metals and Alloys

Chem. Met. Alloys 4 (2011) 152-159
Ivan Franko National University of Lviv
www.chemetal-journal.org

Influence of doping elements (Cu and Fe) on the crystal structure and electrical resistivity of YNi_3 and $Y_{0.95}Ni_2$

O. MYAKUSH[1], V. BABIZHETSKYY[1], P. MYRONENKO[1], H. MICHOR[2], E. BAUER[2], B. KOTUR[1]*

[1] *Department of Inorganic Chemistry, Ivan Franko National University of Lviv, Kyryla i Mefodia St. 6, UA-79005 Lviv, Ukraine*
[2] *Institute of Solid State Physics, Vienna University of Technology, Wiedner Hauptstrasse 8-10, A-1040 Vienna, Austria*
* *Corresponding author. E-mail: kotur@franko.lviv.ua*

Received January 13, 2011; accepted May 18, 2011; available on-line November 8, 2011

Two solid solutions on the basis of the binary compounds YNi_3 and $Y_{0.95}Ni_2$ were investigated by X-ray and electron probe microanalysis for the influence of Fe and Cu-doping on the crystal structure and electrical properties. Substitution of Cu for Ni in YNi_3 does not change the structure type ($PuNi_3$). The replacement of Ni by Cu in $Y_{0.95}Ni_{2-x}Cu_x$ up to $x < 0.15$ and the replacement of Ni by Fe in $Y_{0.95}Ni_{2-x}Fe_x$ up to $x < 0.1$ preserve the structure of the binary parent compound $Y_{0.95}Ni_2$ ($TmNi_2$ structure type, space group *F*-43*m*). Substitution by larger quantities of Cu and Fe destabilizes the $TmNi_2$ superstructure, which converts into the $MgCu_2$ structure with disordered Y vacancies. All the investigated alloys showed metallic-like conductivity following the Nordheim relation.

Yttrium intermetallic compounds / Doping / Crystal structure / Electrical resistivity

1. Introduction

Intermetallic compounds RM_n (*R* = rare earth, *M* = 3*d*-element, *n* = 2 or 3) exhibit a large variety of interesting physical properties. Some of these compounds also absorb large amounts of hydrogen, which induces remarkable changes of their physical properties. Intermetallics and their hydrides attract interest as objects for fundamental investigations and for practical application in the production of magnetic materials, hydrogen accumulators, metal hydride electrodes, *etc.* [1-3].

During the past years we have studied a number of binary RM_2 and RM_3 compounds doped with a third component (*R*' or *M*') with respect to the influence of the doping element on the crystal structure, electrical and magnetic properties and hydrogenation ability of these alloys. The results have been presented in [4-15].

Early reports on binary YNi_2 indicated that it belongs to the cubic $MgCu_2$ Laves phase structure [16]. It was recently shown that YNi_2 crystallizes in a superstructure of the cubic $MgCu_2$ Laves phase structure ($TmNi_2$ structure type) with the nominal composition $Y_{0.95}Ni_2$. This superstructure with space group *F*-43*m* is characterized by ordered Y vacancies in the 4*a* sites and a doubling of the lattice parameter *a* in comparison to the basic $MgCu_2$ structure [17].

Investigations of the electrical resistivity of YNi_2 [18] and of other transport properties (thermal conductivity, thermopower) of the RNi_2 series [1] evidenced anomalies for some of these compounds at high temperatures. Gratz *et al*. [19] later attributed these high-temperature transport anomalies to structural phase transitions from the superstructure type (space group *F*-43*m*) at lower temperatures to the $MgCu_2$ structure type (space group *Fd*-3*m*), stable at higher temperatures. Our previous works [5-9,11-13,15] were focused on the influence of substitution of Fe for Ni, or non-magnetic Y for the magnetic rare earths Er and Gd, on the crystal structure, electrical and magnetic properties, hydrogenation ability and kinetics of the hydrogenation-dehydrogenation process of $R_{0.85}Y_{0.15}Ni_2$ and $RNi_{1.85}Fe_{0.15}$ (*R* = Gd, Er) alloys based on the binary RNi_2 (*R* = Gd, Er) compounds. The results of the crystal structure investigations showed that the parent compound RNi_2 and *R*/Y substituted $R_{0.85}Y_{0.15}Ni_2$ (*R* = Gd and Er) alloys belong to the $TmNi_2$ superstructure type, but the Fe-containing alloys $GdNi_{1.85}Fe_{0.15}$ and $ErNi_{1.85}Fe_{0.15}$ crystallize in the $MgCu_2$-type structure. All the investigated alloys showed metallic-like conductivity and exhibited long-range magnetic order [20]. Transition into a ferromagnetically ordered ground state was also apparent from the resistivity data. All the substituted alloys exhibited anomalies in their

physical properties near the ferromagnetic phase transition temperatures. Increasing order of the magnetic structure with decreasing temperature was revealed by a decrease of the electrical resistivity.

Binary YNi_3 crystallizes in the $PuNi_3$-type rhombohedral structure (space group *R*-3*m*) [21]. The crystal structure of the RNi_3 compounds can be presented as a stacking of RNi_5 ($CaCu_5$ Haucke phase) and RNi_2 ($MgZn_2$ Laves phase) structure fragments [22]. Hydrogen-absorbing RNi_3 intermetallic compounds (*R* = Y and rare earths) have already been known for more than three decades. However, increased interest in these compounds as hydrogen storage materials has appeared in recent years, mainly because of the prospect of electrochemical applications [23]. Among the RNi_3 compounds, YNi_3 displays the highest hydrogen sorption capacity. A partial replacement of Ni by Cr, Mn, Fe, Co, V [24], or Cu [10] decreases its hydrogen sorption capacity.

Single crystals of weakly itinerant ferromagnetic (T_C = 35 K) YNi_3 [25] display a non-Fermi liquid (NLF) temperature dependence of the resistivity. The resistivity does not follow the T^2-law [26], as would be expected from the conventional Fermi liquid theory.

Our previous systematic investigation of the phase equilibria in the Y–Cu–Ni system at 600°C [27,28] has shown the existence of limited solid solutions $Y_{1-\delta}Ni_{2-x}Cu_x$ ($0 < \delta < 0.05$; $0 < x < 0.30$) and $YNi_{3-x}Cu_x$ (x = 0.2 and x = 0.4) based on the binary compounds $Y_{1-\delta}Ni_2$ ($0 \le \delta \le 0.05$) and YNi_3. The present work focuses on investigations of the influence of Cu and Fe as doping elements on the structure and electrical resistivity of the binary compounds $Y_{0.95}Ni_2$ and YNi_3.

2. Experimental details

Alloys were prepared by arc melting of starting elements with a purity not less than 99.9 wt.% under argon. The weight losses were less than 1 % of the total mass of the ingots. The alloys were homogenized in evacuated quartz ampoules at 870 K for 720 h. The samples were examined by X-ray powder diffraction (XRD) using a STOE STADI P diffractometer with Cu K_α-radiation. All the crystal structure calculations were performed by the Rietveld method with the programs FullProf [29] and CSD [30], using the compositions obtained by electron probe microanalysis. Qualitative and quantitative composition analyses on the bulk samples were performed with a scanning electron microscope REMMA-102-2. The temperature dependence of the electrical resistivity was studied by the four probe *a.c.*-bridge method in the temperature range 4-300 K.

3. Results and discussion

The XRD patterns of binary YNi_3 and the pseudo-binary solid solution $YNi_{3-x}Cu_x$ ($0 \le x \le 0.8$) were indexed in the $PuNi_3$-type structure (space group *R*-3*m*) and are presented in Fig. 1. The data show that the replacement of Ni by Cu in YNi_3 does not change the crystal structure of the solid solution. The lattice parameters increase with increasing Cu content (Table 1). The refined final atomic parameters for one alloy of the solid solution, $YNi_{2.2}Cu_{0.8}$, are presented in Table 2.

XRD patterns of the parent $Y_{0.95}Ni_2$ alloy and alloys of the solid solutions $Y_{0.95}Ni_{2-x}Cu_x$ ($0 \le x \le 0.3$)

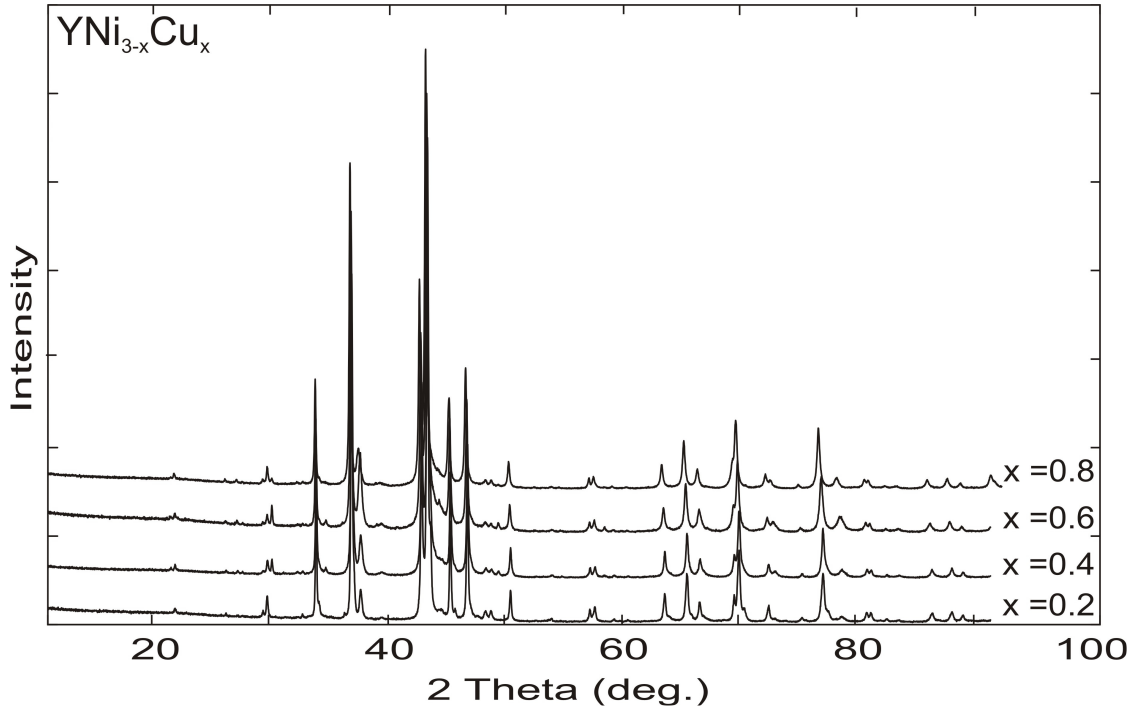

Fig. 1 X-ray powder diffraction patterns of alloys of the solid solution $YNi_{3-x}Cu_x$ ($PuNi_3$-type structure).

Table 1 Lattice parameters of $YNi_{3-x}Cu_x$ ($0 \le x \le 0.8$; $PuNi_3$-type structure, space group *R*-3*m*).

Composition	*a* (nm)	c (nm)	*V* (nm^3)
YNi_3	0.4978(1)	2.4450(1)	0.5247(1)
$YNi_{2.8}Cu_{0.2}$	0.49837(1)	2.4454(1)	0.5258(1)
$YNi_{2.6}Cu_{0.4}$	0.49935(2)	2.4477(1)	0.5285(2)
$YNi_{2.4}Cu_{0.6}$	0.49966(1)	2.4486(1)	0.5293(1)
$YNi_{2.2}Cu_{0.8}$	0.50095(1)	2.4503(1)	0.5324(1)

Table 2 Refined atomic parameters, site occupations (*G*) and isotropic temperature coefficients (B_{iso}) for $YNi_{2.2}Cu_{0.8}$ ($PuNi_3$-type structure, $R_B = 0.0587$).

Atom	Site	*x*	*y*	*z*	*G*	$B_{iso}\times10^2$ (nm^2)
Y1	3*a*	0	0	0	1.0	1.31(5)
Y2	6*c*	0	0	0.14041(9)	1.0	1.07(7)
M1	3*b*	0	0	½	0.753Ni+0.247Cu	1.51(7)
M2	6*c*	0	0	0.33423(18)	0.750Ni+0.250Cu	1.53(11)
M3	18*h*	0.8292(4)	0.1708(4)	0.58390(2)	0.736Ni+0.264Cu	1.32(6)

Table 3 Crystallographic parameters of solid solutions $Y_{0.95}Ni_{2-x}Cu_x$ ($0 \le x \le 0.3$) and $Y_{0.95}Ni_{2-x}Fe_x$ ($0 \le x \le 0.1$).

Composition	Structure type	Space group	*a* (nm)	*V* (nm^3)
$Y_{0.95}Ni_2$[a]	$TmNi_2$	*F*-43*m*	1.4347(2)[a] 1.4357[b]	2.9529(4)[a] 2.959[b]
$Y_{0.95}Ni_{1.97}Cu_{0.03}$	$TmNi_2$	*F*-43*m*	1.43501(1)	2.95486(1)
$Y_{0.95}Ni_{1.92}Cu_{0.08}$	$TmNi_2$	*F*-43*m*	1.43541(1)	2.95881(1)
$Y_{0.95}Ni_{1.85}Cu_{0.15}$	$MgCu_2$	*Fd*-3*m*	0.71723(1)	0.36896(3)
$Y_{0.95}Ni_{1.7}Cu_{0.3}$	$MgCu_2$	*Fd*-3*m*	0.71823(1)	0.37031(2)
$YNi_{1.9}Cu_{0.2}$[b]	$TmNi_2$	*F*-43*m*	1.4368[b]	2.966[b]
$YNi_{1.8}Cu_{0.4}$[b]	$TmNi_2$	*F*-43*m*	1.4369[b]	2.967[b]
$Y_{0.95}Ni_{1.97}Fe_{0.03}$	$TmNi_2$	*F*-43*m*	1.43614(1)	2.96202(7)
$Y_{0.95}Ni_{1.95}Fe_{0.05}$	$TmNi_2$	*F*-43*m*	1.43639(3)	2.9636(2)
$Y_{0.95}Ni_{1.9}Fe_{0.1}$	$MgCu_2$	*Fd*-3*m*	0.71872(1)	0.37126(2)

[a] present data; [b] data from [31]

and $Y_{0.95}Ni_{2-x}Fe_x$ ($0 \le x \le 0.1$) are presented in Figs. 2 and 3. A detailed analysis of the crystal structure of these solid solutions showed that the replacement of Ni by Cu in $Y_{0.95}Ni_{2-x}Cu_x$ up to $x < 0.15$ (< 5 at.% Cu) and the substitution of Ni by Fe in $Y_{0.95}Ni_{2-x}Fe_x$ up to $x < 0.1$ (< 3 at.% Fe) preserve the structure of the binary parent compound $Y_{0.95}Ni_2$ ($TmNi_2$ structure type, space group *F*-43*m*). The presence of superstructure reflections (see Figs. 2 and 3) indicates that all the samples of the solid solution belong to the cubic structure type with doubled cell parameter 2*a* (where *a* is the unit cell parameter of the $MgCu_2$-type structure). The lattice parameters increase with increasing Cu and Fe content (see Table 3). Higher contents of Cu and Fe lead to a phase transition from the $TmNi_2$ superstructure to the $MgCu_2$ structure type. There are no visible superstructure lines in the XRD patterns of $Y_{0.95}Ni_{1.7}Cu_{0.3}$ and $Y_{0.95}Ni_{1.9}Fe_{0.1}$ (see Figs. 2 and 3). However, according to Paul-Boncour *et al.* [31] the pseudo-binary solid solution $Y(Ni,Cu)_2$ adopts the superstructure within the homogeneity range up to about 20 at.% Cu ($x = 0.6$). The difference between the present data and those of [31] may be attributed to the different annealing temperatures applied in the two investigations, 870 K and 1023 K, respectively. Refined lattice parameters of the solid solution series $Y(Ni,Cu)_2$ are summarized in Table 3. The atomic parameters of $Y_{0.95}Ni_{1.92}Cu_{0.08}$ ($TmNi_2$-type structure) and $Y_{0.95}Ni_{1.7}Cu_{0.3}$ ($MgCu_2$-type structure) alloys are presented in Tables 4 and 5.

Electrical resistivity measurements were carried out to supplement the crystallographic studies by the information revealed from the scattering of conduction electrons in the investigated solid solutions In solid solutions of fully miscible isostructural nonmagnetic elements, *e.g.* alloys of the noble metals Ag and Au, the low-temperature resisitivities are dominated by disorder scattering of the conduction electrons. Accordingly, the residual resistivities of the solid solution $Au_{1-x}Ag_x$ follow the simple Nordheim relation, $\rho_0(x) = C{\cdot}x(1\text{-}x)$ [32]. Deviations of $\rho_0(x)$ from the Nordheim rule are expected in the presence

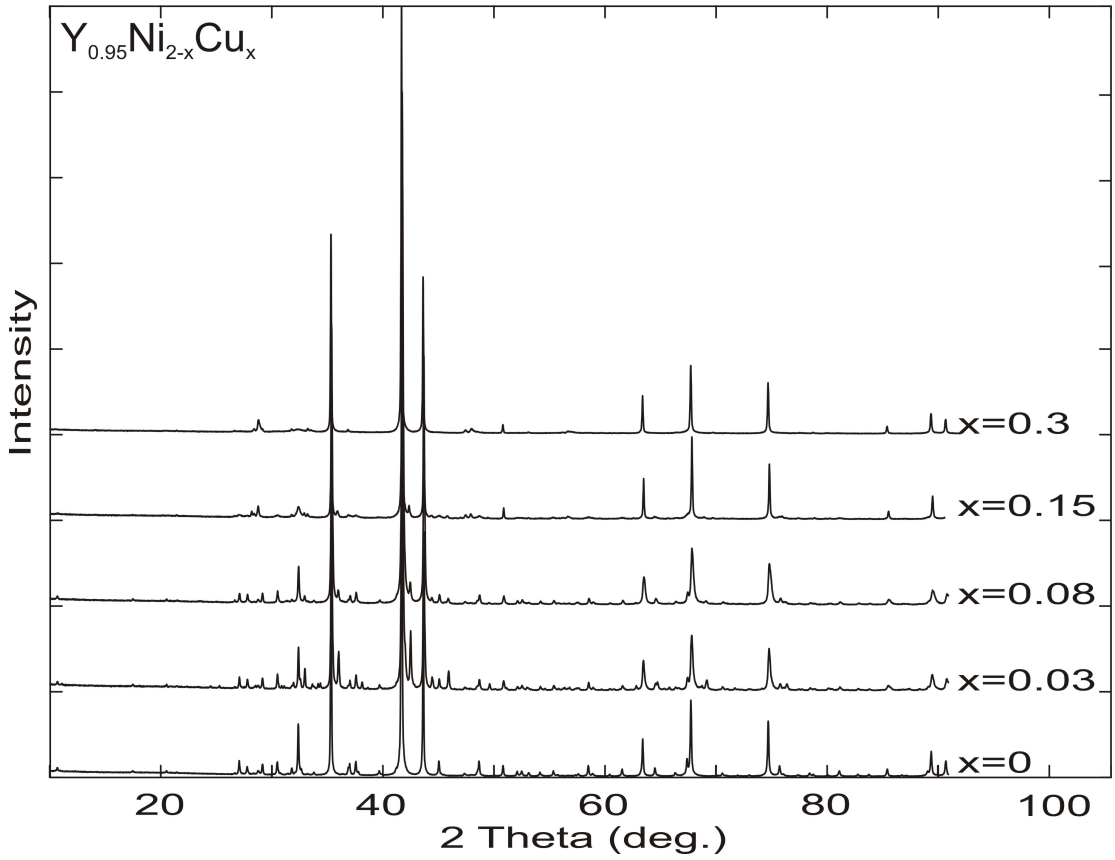

Fig. 2 X-ray powder diffraction patterns of alloys of the solid solution $Y_{0.95}Ni_{2-x}Cu_x$.

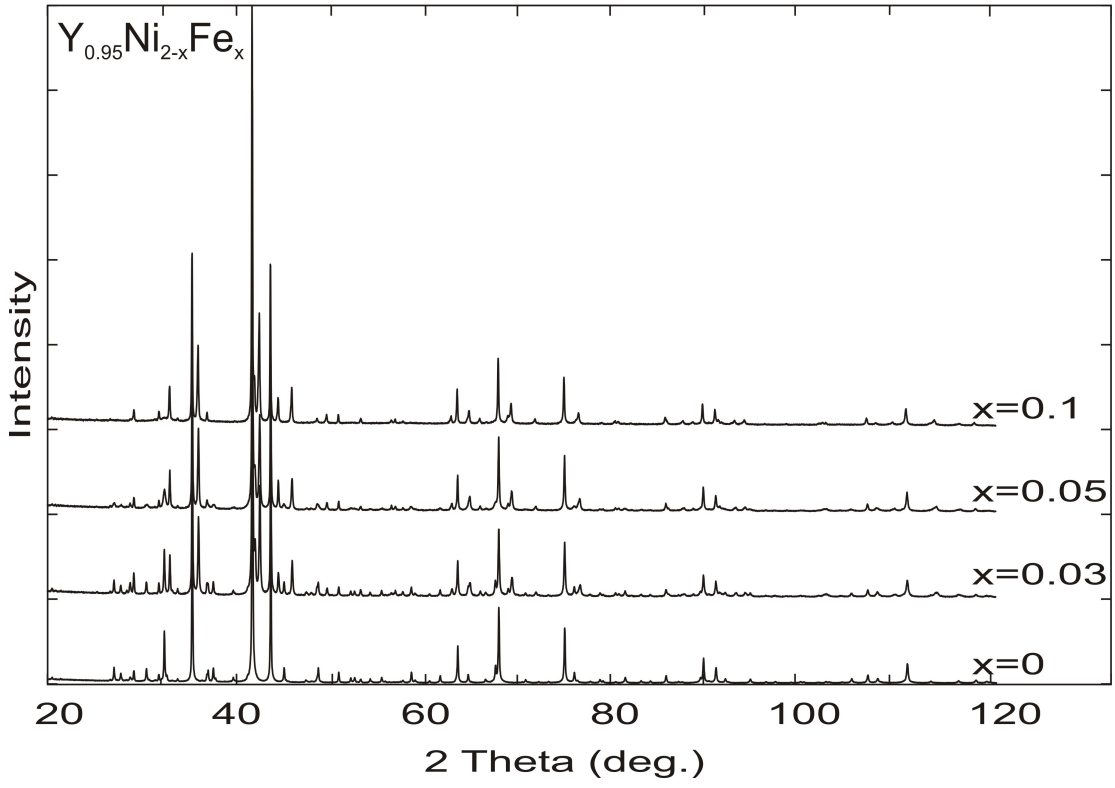

Fig. 3 X-ray powder diffraction patterns of alloys of the solid solution $Y_{0.95}Ni_{2-x}Fe_x$.

Table 4 Refined atomic parameters, site occupation (G) and isotropic temperature coefficients (B_{iso}) for $Y_{0.95}Ni_{1.92}Cu_{0.08}$ ($TmNi_2$-type structure, R_B = 0.052).

Atom	Site	x	y	z	G	$B_{iso}\times10^2$ (nm^2)
Y1	4*a*	0	0	0	0.401(8)	1.49(1)
Y2	4*b*	½	½	½	1.0	0.65(1)
Y3	16*e*	0.10308(5)	*x*	*x*	1.0	0.69(1)
Y4	16*e*	0.62606(7)	*x*	*x*	1.0	0.52(1)
Y5	24*g*	0.0078(1)	¼	¼	1.0	0.93(1)
M1	16*e*	0.3118(2)	*x*	*x*	0.96 Ni + 0.04 Cu	0.52(1)
M2	16*e*	0.8118(2)	*x*	*x*	0.96 Ni + 0.04 Cu	0.99(1)
M3	48*h*	0.0654(1)	*x*	0.8089(2)	0.96 Ni + 0.04 Cu	0.57(1)
M4	48*h*	0.0619(1)	*x*	0.3118(2)	0.96 Ni + 0.04 Cu	0.61(1)

Table 5 Refined atomic parameters, site occupation (G) and isotropic temperature coefficients (B_{iso}) for $Y_{0.95}Ni_{1.7}Cu_{0.3}$ ($MgCu_2$-type structure, R_B = 0.032).

Atom	Site	x	y	z	G	$B_{iso}\times10^2$ (nm^2)
Y	8*b*	⅜	⅜	⅜	0.95	1.06(1)
M	16*c*	0	0	0	0.85 Ni + 0.15 Cu	1.04(1)

of magnetic elements and, in particular, for solid solutions undergoing changes of their crystal structures and/or magnetic ground states.

Temperature dependent electrical resistivities, $\rho(T)$, of polycrystalline samples of the binary parent compound YNi_3 and the solid solutions $YNi_{3-x}Cu_x$ (x = 0.2, 0.4, 0.6, and 0.8) are displayed in Fig. 4a. The resistivities $\rho(T)$ of all the samples in this series exhibit a rather simple, metallic-like temperature dependence. Only in the case of weakly ferromagnetic YNi_3 the resistivity data exhibit a sharp kink at about 32 K, which indicates a phase transition to a ferromagnetic ground state (previously reported by Gignoux *et al.* [25]). The present results obtained for polycrystalline YNi_3 are in reasonable agreement with the earlier single-crystal studies [25]. The substitution of Cu for Ni is expected to weaken and eventually suppress long-range ferromagnetic order. The evolution of the composition dependence of the residual resistivity $\rho_0(x)$, *i.e.* the resitivity values ρ(4.2 K) of each composition $YNi_{3-x}Cu_x$, collected in Fig. 4b, reveals a marked increase of ρ_0 from YNi_3 to $YNi_{2.8}Cu_{0.2}$ by about 35 μΩ cm, but a significantly smaller variation of $\rho_0(x)$ within the solid solution $YNi_{3-x}Cu_x$, which approximately follows a modified Nordheim rule, $\rho_0(x) = A + C{\cdot}x(3-x)$, where A is a constant off-set and C the factor for disorder scattering in the (Ni,Cu) sublattice. The dashed line in Fig. 4b shows a fit using the Nordheim rule, which yields $A \approx 40$ μΩ cm and $C \approx 20$ μΩ cm. The 40 μΩ cm off-set of the residual resistivities of the Cu doped samples most likely originates from incoherent magnetic scattering of the conduction electrons, *i.e.* some kind of spin disorder scattering induced by substitutional disorder, which suppresses the long-range ferromagnetic order of the parent compound YNi_3.

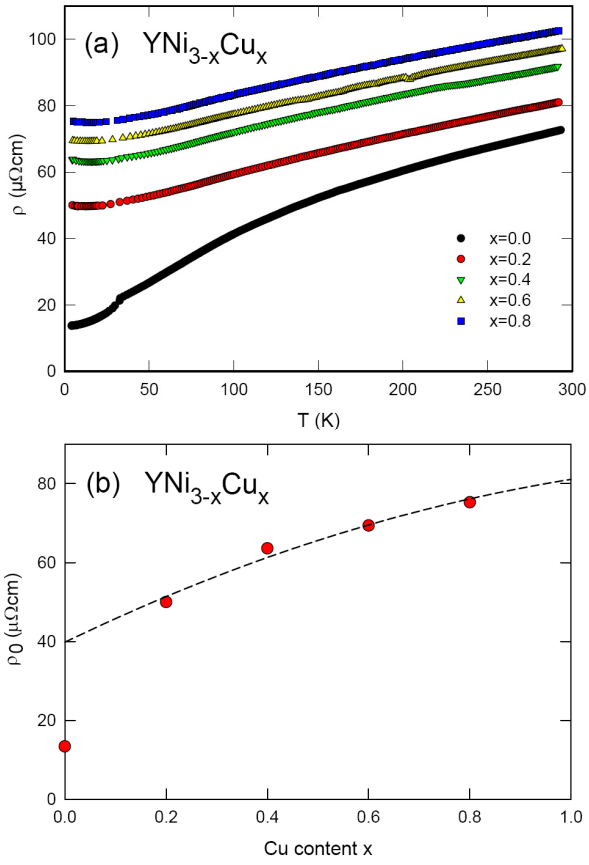

Fig. 4 Temperature dependent electrical resistivity $\rho(T)$ (a) and composition dependent residual resistivity $\rho_0(x)$ (b) of solid solutions $YNi_{3-x}Cu_x$; the dashed line shows a fit according to the Nordheim rule.

In case of the solid solution $Y_{0.95}Ni_{2-x}Cu_x$, all the compositions, including the binary parent compound $Y_{0.95}Ni_2$, show Pauli paramagnetic ground state and the electrical resistivities displayed in Fig. 5a exhibit a simple metallic temperature dependence, which is dominated by the scattering of conduction electrons on static lattice defects and phonons and consequently follows the simple Bloch-Grüneisen (BG) law

$$\rho(T) = \rho_0 + B\frac{T^5}{\Theta_D^6}\int_0^{\Theta_D/T}\frac{x^5}{(e^x-1)(1-e^{-x})}dx,$$

yielding the values of residual resistivity shown in Fig. 5b, moderate variations of the Debye temperature $\Theta_D \approx 220 \pm 30$ K and an electron-phonon coupling factor B in the range 6-10 mΩ cm K. The moderate reduction of the temperature dependence of the resitivity of $Y_{0.95}Ni_{1.7}Cu_{0.3}$ is attributed to the larger absolute resistivity exceeding 150 μΩ cm, which leads to deviations from the Matthiessen rule and consequently to a flattening of $\rho(T)$ (see *e.g.* [33]). The residual resistivity, $\rho_0(x)$, of $Y_{0.95}Ni_{2-x}Cu_x$ in Fig. 5b reveals a significant discontinuity within the series, *i.e.* a marked increase of ρ_0 between $Y_{0.95}Ni_{1.92}Cu_{0.08}$ and $Y_{0.95}Ni_{1.85}Cu_{0.15}$, which coincides with the vanishing of the superstructure reflections in Fig. 2, *i.e.* with the change of the crystal structure from the $TmNi_2$ type to the $MgCu_2$ type. The different trends of $\rho_0(x)$ in the $TmNi_2$-type and $MgCu_2$-type ranges of the solid solution $Y_{0.95}Ni_{2-x}Cu_x$ are emphasized by dashed and dotted lines [Nordheim fits, $\rho_0(x) = A + C{\cdot}x(2\text{-}x)$], respectively. According to these fits, the loss of the superstructure ordering of Y vacancies is accompanied by an increase of the A parameter from 10 μΩ cm to 22 μΩ cm and an increase of the factor C from 140 μΩ cm to 225 μΩ cm. Magnetic effects do not seem to play any role in the solid solution $Y_{0.95}Ni_{2-x}Cu_x$, because all the samples remain paramagnetic.

The most significant changes of the electrical resistivity are observed in the solid solution $Y_{0.95}Ni_{2-x}Fe_x$ (see Fig. 6). Only the binary parent compound $Y_{0.95}Ni_2$ exhibits a simple BG-like metallic behavior (as mentioned above), whereas the Fe-doped solid solutions initially display an one order of magnitude stronger increase of the residual resistivity ρ_0 as compared to $Y_{0.95}(Ni,Cu)_2$ and $Y(Ni,Cu)_3$, and also a marked increase of the slope of $\rho(T)$ at the lowest temperatures with an approximate T-linear temperature dependence. At higher Fe contents the residual resistivity drops and for $Y_{0.95}Ni_{1.7}Fe_{0.3}$ the low-temperature behavior has changed back to the more common T-square dependence. The Fe-richest composition $Y_{0.95}Ni_{1.5}Fe_{0.5}$ exhibits a kink in $\rho(T)$ at about 80 K. All these marked changes refer to magnetic effects caused by the Fe doping, which may initially lead to a magnetic spin or cluster glass ground state (for $Y_{0.95}Ni_{2-x}Fe_x$, x = 0.05 and 0.1), and eventually to long-range ferromagnetic order, which is in line with the T^2 dependence of $Y_{0.95}Ni_{1.7}Fe_{0.3}$ and $Y_{0.95}Ni_{1.5}Fe_{0.5}$ and explains, in particular, the kink in $\rho(T)$ observed for the latter. More detailed magnetic studies are in progress to clarify the magnetic ground states in the solid solution series $Y_{0.95}Ni_{2-x}Fe_x$.

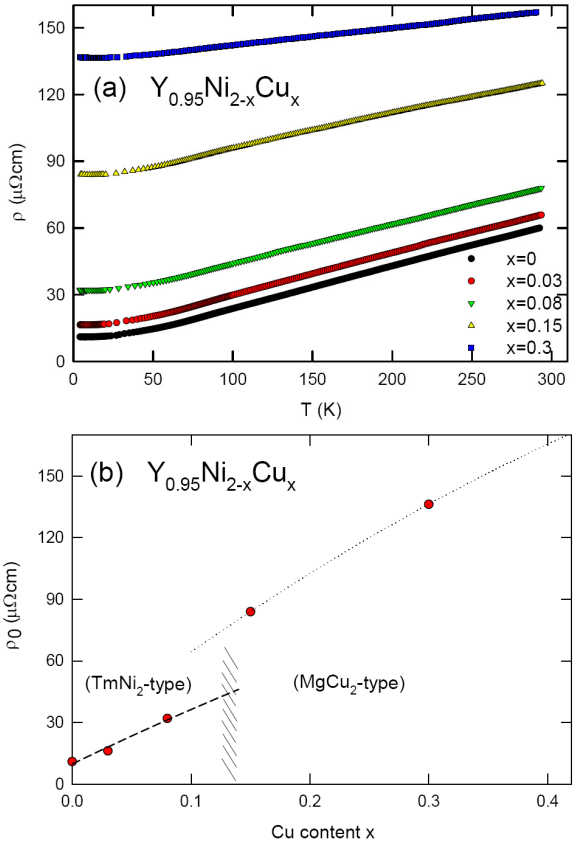

Fig. 5 Temperature dependent electrical resistivity $\rho(T)$ (a) and composition dependent residual resistivity $\rho_0(x)$ (b) of solid solutions $Y_{0.95}Ni_{2-x}Cu_x$; the dashed and dotted lines indicate fits according to the Nordheim rule for the $TmNi_2$-type and $MgCu_2$-type solid solutions, respectively.

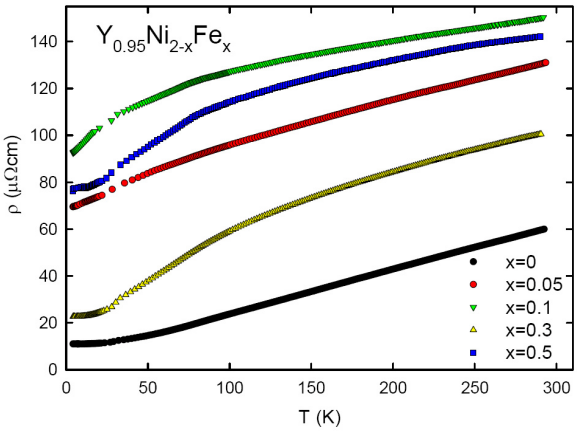

Fig. 6 Temperature dependent electrical resistivity of solid solutions $Y_{0.95}Ni_{2-x}Fe_x$.

4. Conclusions

Substitution of Cu for Ni in the binary compound YNi_3 ($PuNi_3$-type structure, space group *R*-3*m*) results in the existence of a limited solid solution $YNi_{3-x}Cu_x$ ($0 \le x \le 0.8$). The lattice parameters increase with increasing Cu content. The replacement of Ni by small quantities of Cu in $Y_{0.95}Ni_{2-x}Cu_x$ up to $x < 0.15$ and substitution of Fe for Ni in $Y_{0.95}Ni_{2-x}Fe_x$ up to $x < 0.1$ preserve the structure of the binary parent compound $Y_{0.95}Ni_2$ ($TmNi_2$ structure type). The replacement of Ni by larger quantities of Cu and Fe destabilizes the $TmNi_2$ superstructure, which converts into the $MgCu_2$ structure with a constant amount of Y vacancies.

The results of the electrical resistivity measurements of the Cu-doped solid solutions are mostly in line with the usual substitutional disorder effect as suggested by the Nordheim rule. Deviations from the simple Nordheim-type variation of the residual resistivity are clearly connected to the loss of weak ferromagnetic order in the solid solution $YNi_{3-x}Cu_x$ and to the loss of superstructure ordering in $Y_{0.95}Ni_{2-x}Cu_x$. In the case of the solid solution $Y_{0.95}Ni_{2-x}Fe_x$, large changes of the temperature dependent electrical resistivity are observed and refer to effects of Fe magnetism, which for lower Fe concentrations is most likely of the spin glass type and long-range ferromagnetic for larger Fe contents.

References

[1] J.M. Fournier, E. Gratz, In: K.A. Gschneidner Jr., L. Eyring, G.H. Lander, G.R. Choppin (Eds), *Handbook on the Physics and Chemistry of Rare Earths*, Vol. 17, Amsterdam: North-Holland, 1993, p. 409.

[2] K. Yvon, P. Fischer, In: Louis Schlapbach (Ed.), *Topics in Applied Physics, Vol. 63. Hydrogen in Intermetallic Compounds I. Electronic, Thermodynamic, and Crystallographic Properties, Preparation*, Springer-Verlag, Berlin, 1988, pp. 87-138.

[3] G. Wiesinger, G. Hilscher, In: K.H.J Buschow (Ed.), *Handbook on Magnetic Materials*. Vol. 17, Elsevier B.V., Amsterdam, 2008, pp. 293-456

[4] O. Myakush, Yu. Verbovytsky, I. Saldan, I. Kovalchuck, I. Zavalii, B. Kotur, *Mater. Sci.* 40 (2004) 781-786.

[5] O. Myakush, Yu. Verbovytsky, B. Kotur, I. Kovalchuck, V. Beresovetz, I. Zavaliy, *J. Phys.: Conf. Ser.* 79 (2007) 012018.

[6] O.R. Myakush, Yu.V. Verbovytskyi, V.V. Berezovets, O.H. Ershova, V.D. Dobrovolskyi, B.Ya. Kotur, *Mater. Sci.* 43 (2007) 682-688.

[7] B. Kotur, O.Myakush, I. Zavaliy, *J Alloys Compd*. 442 (2007) 17-21.

[8] O.R. Myakush, Y.V. Verbovytsky, I.V. Koval'chuck, R.V. Denys, V.V. Berezovets, B.Ya. Kotur, *Abstr. X Int. Conf. Cryst. Chem. Intermet. Compd.*, Lviv, Ukraine, 2007. p. 97.

[9] B. Kotur, Yu. Verbovytsky, O. Myakush, I. Kovalchuk, V. Berezovets, *Abstr. Int. Conf. Solid Compd. Transition Elem.*, Dresden, 2008. p. 344.

[10] O. Myakush, Yu. Verbovytsky, O. Myagkota, I. Koval'chuk, V. Berezovets', I. Zavaliy, *Visn. Lviv. Univ., Ser. Khim.* 49 (2008) 128-136.

[11] B. Kotur, O. Myakush, I. Zavaliy, *Croat. Chem. Acta* 82 (2009) 469-476.

[12] H. Michor, B. Kotur, O. Myakush, G. Hilscher, *Abstr. XV Int. Semin. Phys. Chem. Solids*, Szklarska Poręba, Poland. 2009, p. 27.

[13] B. Kotur, O. Myakush, H. Michor, E. Bauer, *J. Alloys Compd.* 499 (2010) 135-139.

[14] O. Myakush, H. Michor, G. Hilscher, N. Pyk, P. Myronenko, I. Koval'chuk, B. Kotur, *Abstr. XI Int. Conf. Cryst. Chem. Intermet. Compd.*. Lviv, Ukraine, 2010, p. 154.

[15] E. Bauer, O. Myakush, H. Michor, B. Kotur, *Abstr. XVI Int. Semin. Phys. Chem. Solids*, Lviv, Ukraine, 2010. 51-52.

[16] R.H. Van Essen, K.H.J. Buschow, *J. Less-Common Met.* 70 (1980) 189-198.

[17] M. Latroche, V. Paul-Boncour, A. Perchéron-Guègan, J.C. Achard, *J. Less-Common Met.* 161 (1990) L27-L31.

[18] A. Slebarski, *J. Less-Common Met.* 141 (1988) L1-L7.

[19] E. Gratz, A. Kottar, A. Lindbaum, M. Mantler, M. Latroche, V. Paul-Boncour, M. Acet, Cl. Barner, W.B. Holzapfel, V. Pacheco, K. Yvon, *J. Phys.: Condens. Matter.* 8 (1996) 8351-8361.

[20] H. Michor, B. Kotur, O. Myakush, G. Hilscher, *J. Phys.: Conf. Ser.* 289 (2011) 012018.

[21] D.T. Cromer, C.E. Olsen, *Acta Crystallogr.* 12 (1959) 689.

[22] B.D. Dunlap, P.J. Viccaro, G.K. Shenoy, *J. Less-Common Met.* 74 (1980) 75.

[23] M. Latroche, A. Perchéron-Guégan, *J. Alloys Compd.* 356-357 (2003) 461-468.

[24] X. Zhang, W. Yin, Y. Chai, M. Zhao, *Mater. Sci. Eng. B* 117 (2005) 123-128.

[25] D. Gignoux, R. Lemaire, P. Molho, F. Tasset, *J. Magn. Magn. Mater.* 21 (1980) 307-315.

[26] M.J. Steiner, F. Beckers, P.G. Niklowitz, G.G. Lonzarich, *Physica B* 329-333 (2003) 1079-1080.

[27] N. Pyk, P. Myronenko, N. Bykalovich, O. Myakush, B. Kotur, *Visn. Lviv. Univ., Ser. Khim.* 51 (2010) 79-87.

[28] N. Bykalovich, N. Pyk, P. Myronenko, O. Myakush, B. Kotur, *Abstr. XVI Int. Semin. Phys. Chem. Solids*, Lviv, Ukraine, 2010, p. 58.

[29] J. Rodrigues-Carvajal, *Program FullProf*, Lab. Léon Brillouin, CEA-CNRS, 1998.

[30] L.G. Akselrud, P.Yu. Zavalii, Yu.N. Grin, V.K. Pecharsky, B. Baumgartner, E. Wolfel, *Mater. Sci. Forum* 133-136 (1993) 335-340.
[31] V. Paul-Boncour, A. Lindbaum, E. Gratz, E. Leroy, A. Perchėron-Guėgan, *Intermetallics* 10 (2002) 1011-1017.
[32] T.H. Davis, J.A. Rayne, *Phys. Rev. B* 6 (1972) 2931-2942.
[33] J.H. Mooij, *Phys. Status Solidi A* 17 (1973) 521-530.